New Physics: Sae Mulli,
Vol. 74, No. 12, December 2024, pp. 1251∼1257
http://dx.doi.org/10.3938/NPSM.74.1251

Eikonal Model Analysis of $\alpha + {}^{32}$S and $\alpha + {}^{58}$Ni Elastic Scatterings at 386 MeV

Yong Joo Kim*
Department of Physics, Jeju National University, Jeju 63243, Korea

(Received 2 September 2024 : revised 16 October 2024 : accepted 11 November 2024)

The differential cross sections of 386 MeV $\alpha-$particles elastic scattering on ^{32}S and ^{58}Ni are analyzed within the framework of the eikonal model using the tangential velocity at the distance of closest approach. The calculation results successfully reproduce the structure of the experimental angular distributions, and are in good agreement with the measured data. The oscillatory structures observed around the crossing angle in angular distributions are explained in terms of the strong interference between the near-side and the far-side scattering amplitudes. The effect of using tangential velocity on the differential and reaction cross sections is investigated. Furthermore, the critical angular momentum, the strong absorption radius and the reaction cross section are examined.

Keywords: Elastic scattering, Eikonal model, Tangential velocity, $\alpha + {}^{32}$S, $\alpha + {}^{58}$Ni

I. INTRODUCTION

Elastic scattering between heavy-ions (HI) has been one of research topics in nuclear physics over the past decades. The main observation quantity in HI elastic scattering experiment is differential scattering cross section. This physical quantity is theoretically obtained from the square of the scattering amplitude. Meanwhile, the scattering matrix element is a factor that constitutes the scattering amplitude, and is closely related to the nuclear phase shift. Therefore, an important ingredient in calculating the differential scattering cross section is the nuclear phase shift. The eikonal model is a convenient and useful approach to describe the HI elastic scattering cross section in the incident energy range from several tens of MeV/nucleon to about 100 MeV/nucleon. The nuclear phase shift in this model is obtained by integrating the nuclear potential. There have been many studies [1–8] attempting to describe HI elastic scattering using the eikonal model. Trajectory corrections using the effective impact parameters in HI elastic scattering are discussed [5]. In our work [6] conducted a long time ago, analysis of ^{16}O + ^{16}O elastic angular distribution data at incident energies of 480 and 704 MeV was performed using the second-order eikonal model. Elastic scattering of 240 MeV ^{6}Li ions by ^{24}Mg and ^{28}Si was analyzed [7] using an eikonal model that takes into account the tangential velocity at the distance of closest approach.

Elastic scattering between $\alpha-$particle and various target nuclei has been actively studied [9–13]. Nayak *et al.* [11] measured the α + ^{58}Ni elastic scattering cross section at 386 MeV, and used a folding model to describe these data. The measured data of α + ^{32}S system were also obtained [12] at the same incident energy, and analyzed using the DWBA. It is interesting to analyze the measured data of 386 MeV $\alpha-$particles elastic scattering on ^{32}S and ^{58}Ni using the eikonal model. In this paper, we analyze these experimental data using the eikonal model considering the tangential velocity at the distance of closest approach. It is also investigated how the use of tangential velocity affects the results of differential and reaction cross sections calculations. Furthermore, the structure of angular distributions, the Argand diagram of scattering matrix element, the strong absorption radius, the density overlap of two colliding nuclei determined by strong absorption radius, and the

*Correspondence to: yjkim@jejunu.ac.kr

effect of variation in potential radius parameters on the differential and reaction cross sections are investigated.

II. THEORY

The elastic scattering amplitude $f(\theta)$ is expressed as the sum of Rutherford scattering amplitude ($f_R(\theta)$) and nuclear scattering amplitude (second term in the equation below), given as follows:

$$f(\theta) = f_R(\theta) + \frac{1}{2ik}\sum_{L=0}^{\infty}(2L+1)\exp(2i\sigma_L)(S_L-1)P_L(\cos\theta), \quad (1)$$

where $k = \sqrt{2\mu E}/\hbar$, and θ is the scattering angle. Here Coulomb phase shift σ_L, nuclear scattering matrix elements S_L, and Legnedre polynomial $P_L(\cos\theta)$ depend on the orbital angular momentum quantum number L. The S_L has a relationship given by the following equation with the nuclear phase shift δ_L

$$S_L = \exp[2i\delta_L], \quad (2)$$

where δ_L has a complex form. Then, the elastic differential cross section, called angular distribution, is calculated as

$$\frac{d\sigma}{d\Omega} = |f(\theta)|^2. \quad (3)$$

In the eikonal model based on the Coulomb trajectory of colliding nuclei, the nuclear phase shift $\delta_L(r_c)$ is expressed as an integral over the nuclear potential $U(r)$ as follows [3]

$$\delta_L(r_c) = -\frac{1}{\hbar v}\int_0^{\infty} U(r)dz. \quad (4)$$

Here $v = \hbar k/\mu$ is the asymptotic velocity, $r = \sqrt{r_c^2 + z^2}$, and the r_c is the distance of closest approach for a Coulomb trajectory given by [14]

$$r_c = a_c + \sqrt{a_c^2 + b^2}, \quad (5)$$

where $a_c = Z_1 Z_2 e^2/2E$ is the Coulomb length parameter and $b = (L+1/2)/k$ is the impact parameter. In the Coulomb trajectory, the straight-line trajectory is deflected around r_c due to the Coulomb field between the two colliding nuclei. Thus, we will use the tangential velocity considering the deflected trajectory at r_c, and the tangential velocity v_c is given as follows [5]

$$v_c = \frac{b}{r_c}v. \quad (6)$$

If v is replaced by v_c in Eq. (4), the nuclear phase shift $\delta_L(r_c)$ can be written as follows

$$\delta_L(r_c) = -\frac{1}{\hbar v_c}\int_0^{\infty} U(\sqrt{r_c^2 + z^2})dz. \quad (7)$$

In this study, the nuclear phase shift given by Eq. (7) is used instead of Eq. (4). As the $U(r)$, we use six-parameters Woods-Saxon (WS) potential given as follows:

$$U(r) = -V_0\ f(r, r_v, a_v) - iW_0\ f(r, r_w, a_w), \quad (8)$$

where V_0 (W_0) is the real (imaginary) nuclear potential depth, and the form factor $f(r, r_x, a_x)$ is usually taken as

$$f(r, r_x, a_x) = \left[1 + \exp\left(\frac{r - r_x(4^{1/3} + A^{1/3})}{a_x}\right)\right]^{-1}, \quad x = v,\ w. \quad (9)$$

In this equation r_x (a_x) denotes the radius (diffuseness) parameter, where $x = v$ (w) represents the real (imaginary) part, while A is the target mass number. The potential parameters given in Eqs. (8) and (9) are determined by the minimum $\chi^2/N-$fit to the measured data.

III. RESULTS AND DISCUSSION

1. Angular distributions

The elastic scattering cross sections of $\alpha + {}^{32}$S and $\alpha + {}^{58}$Ni systems at 386 MeV were calculated using the eikonal model considering the v_c at r_c. The WS potential parameters that best describe the measured data [11,12] when using Eq. (7) are listed in Table 1 and the corresponding angular distributions are shown as solid curves in Fig. 1. The dotted curves in this figure are the results of using the asymptotic velocity (v) instead of the tangential velocity (v_c) in Eq. (7). Although the two curves show relatively good agreement in the small $\theta_{\rm c.m.}$ regions, it can be seen that there is a substantial difference between the solid curve and the dotted curve in the large

Table 1. Potential parameters extracted from the minimum $\chi^2/N-$fit to the measured data and corresponding $\chi^2/N-$value in the eikonal model analysis using the tangential velocity at r_c for 386 MeV $\alpha-$particle elastic scatterings from ^{32}S and ^{58}Ni. σ_R in the last column is the reaction cross section obtained using the partial wave sum given by Eq. (10). Values in parentheses are the results obtained using the asymptotic velocity. $\chi^2/N-$values were obtained under the assumption that all experimental data have a 10% error.

Target	V_0 (MeV)	r_v (fm)	a_v (fm)	W_0 (MeV)	r_w (fm)	a_w (fm)	χ^2/N	σ_R (mb)
^{32}S	63.7	0.883	0.843	29.6	0.991	0.671	1.33 (4.84)	1052 (1048)
^{58}Ni	74.8	0.916	0.834	33.5	1.022	0.756	1.83 (3.30)	1539 (1532)

Table 2. Same as Table 1, but potential parameters that best fit the measured data when using the asymptotic velocity. $\chi^2/N-$values were obtained under the assumption that all experimental data have a 10% error.

Target	V_0 (MeV)	r_v (fm)	a_v (fm)	W_0 (MeV)	r_w (fm)	a_w (fm)	χ^2/N	σ_R (mb)
^{32}S	75.4	0.836	0.909	34.2	1.003	0.622	2.17	1067
^{58}Ni	85.3	0.883	0.883	40.1	1.014	0.700	2.11	1510

$\theta_{\rm c.m.}$ regions. The solid curves reproduce successfully the complex behavior of experimental angular distribution and give good agreement with the elastic data [11,12] in the entire measured angle regions. The $\chi^2/N-$values obtained from the calculations using v and v_c at r_c, respectively, are shown in Table 1. As this Table shows, the $\chi^2/N-$values using tangential velocity at r_c are reasonable for each scattering system.

In order to compare the degree of agreement with the experimental data [11,12] in the calculation results of the eikonal model considering the v and v_c, the optimal potential parameters that best fit the measured data were found when using the asymptotic velocity, and the values found are shown in Table 2. The eikonal model calculation results using asymptotic velocity and potential parameters given in Table 2 are shown as dashed curves in Fig. 1. As shown in Tables 1 and 2, the $\chi^2/N-$values of the calculation results using the tangential velocity are smaller than the results using the asymptotic velocity. This means that the solid curves of Fig. 1 match the measured data better than the dashed curves.

The technique of decomposing the $f(\theta)$ into near- and far-sides using the Fuller formalism [15] helps to qualitatively understand the structure of the angular distribution. The contributions of the near-side and far-side components to the $d\sigma/d\sigma_{\rm Ruth}$ obtained from the eikonal model using v_c at r_c are shown as dotted and dashed curves, respectively, in Fig. 2 along with the $d\sigma/d\sigma_{\rm Ruth}$ shown as solid curves. The near-side cross sections dominate at small scattering angles, while the far-side cross sections contribute little. However, the far-side contributions increase in magnitude as the $\theta_{\rm c.m.}$ increases and become equal to the near-side contributions at crossing angle $\theta_{\rm cross}$ ($\theta_{\rm cross} = 3.30^\circ$ for $\alpha + {}^{32}$S and $\theta_{\rm cross} = 4.50^\circ$ for $\alpha + {}^{58}$Ni). At scattering angles larger than the $\theta_{\rm cross}$, the near-side amplitude does not contribute significantly, while the far-side amplitude makes an important contribution in determining the behavior of the elastic cross section. The strong interference between the near- and far-side scattering amplitudes can be thought of as giving rise to an oscillating structure observed around the $\theta_{\rm cross}$.

2. Scattering Matrix Elements and Reaction Cross Sections

Argand diagrams of the scattering matrix elements S_L using eikonal phase shift given by Eq. (7) are plotted in Fig. 3. The Arabic numerals along the curve in this figure represent the values of orbital angular momentum quantum number L. The Argand diagrams of two scattering systems show similar shapes. This graphical images of S_L shows two distinct characteristics. The first one is that they starts at (Re(S_L), Im(S_L)) = (0.0, 0.0) and finally end at (1.0, 0.0). The other is that the graphical image

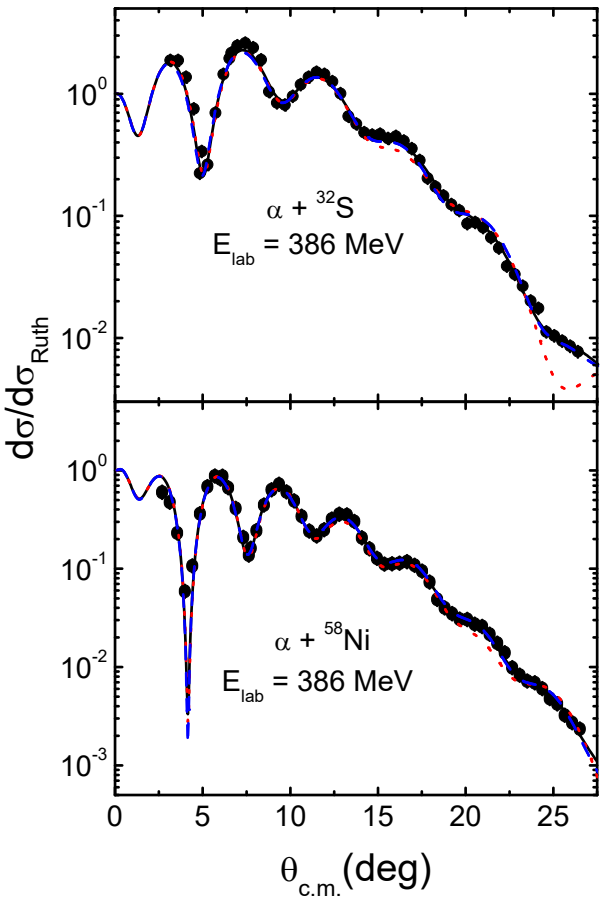

Fig. 1. (Color online) Angular distributions for the elastic scattering of 386 MeV $\alpha-$particles from ^{32}S and ^{58}Ni. The solid curves are the eikonal model calculations using tangential velocity whereas the dotted curves are the calculations using asymptotic velocity, where both results were calculated using the WS potential parameters given in Table 1. The dashed curves are the calculation results that best fits the experimental data when using the asymptotic velocity, and the potential parameters used are shown in Table 2. Experimental data are taken from Refs. 11,12.

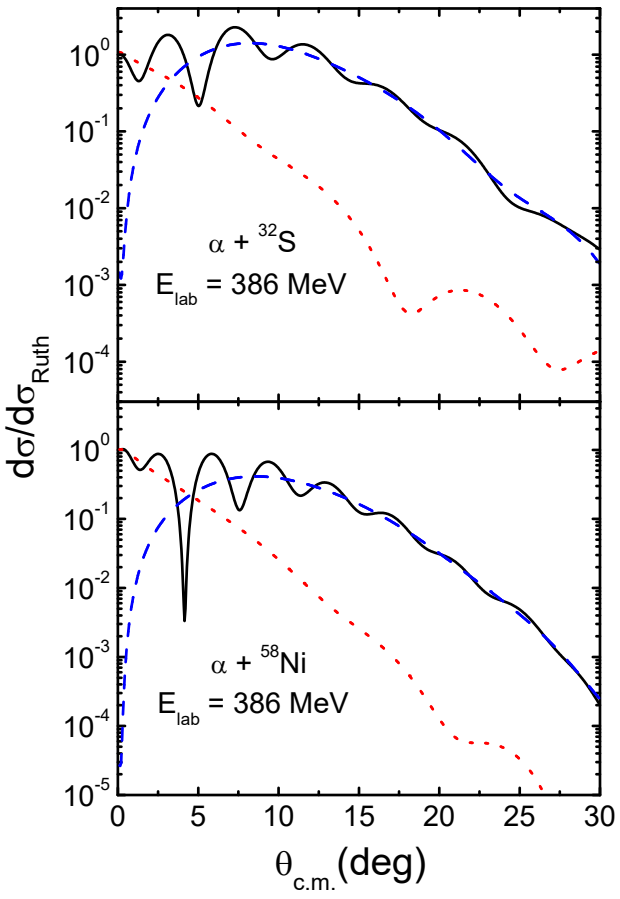

Fig. 2. (Color online) Differential cross sections (solid curves) drawn as solid curves in Fig. 1 for the elastic scattering of 386 MeV $\alpha-$particles from ^{32}S and ^{58}Ni, their near-side (dotted curves) and far-side (dashed curves) components calculated from the Fuller's formalism [15].

depicts the shape of a nautilus shell spiral, as shown in Fig. 3.

The transmission functions $T_L = 1 - |S_L|^2$ using Eqs. (2) and (7) are plotted in Fig. 4(a). The T_L functions have a value of 1 for small L and 0 for large L, and change rapidly from 1 to 0 around the critical angular momenta $L_{1/2}$ (42.44 for α + ^{32}S and 54.17 for α + ^{58}Ni) corresponding to $T_L = 0.5$. The $L_{1/2}$ is closely related to the strong absorption radius R_s defined as $R_s = a_c + \sqrt{a_c^2 + (L_{1/2} + \frac{1}{2})^2/k^2}$. The calculated R_s values are 5.688 fm for α + ^{32}S and 6.912 fm for α + ^{58}Ni systems, respectively. Furthermore, using the R_s, the so-called geometric reaction cross section can be calculated from the relationship $\sigma_{R_s} = \pi R_s^2$, and the obtained values are 1017 mb and 1501 mb for ^{32}S and ^{58}Ni targets, respectively. Meanwhile, the reaction cross section σ_R given in Tables 1 and 2 is obtained using the partial wave sum given by

$$\sigma_R = \frac{\pi}{k^2} \sum_{L=0}^{\infty} (2L+1) T_L, \qquad (10)$$

where T_L is the transmission function mentioned just before. From the σ_R values given in Table 1, the following three facts can be known. First, the σ_R obtained using tangential velocity is slightly larger than that obtained using asymptotic velocity. Second, the σ_{R_s} value for each scattering system is similar to the σ_R ones, which indicate that R_s provides quite a satisfactory account of the σ_R obtained using partial wave sum. Third, as the tar-

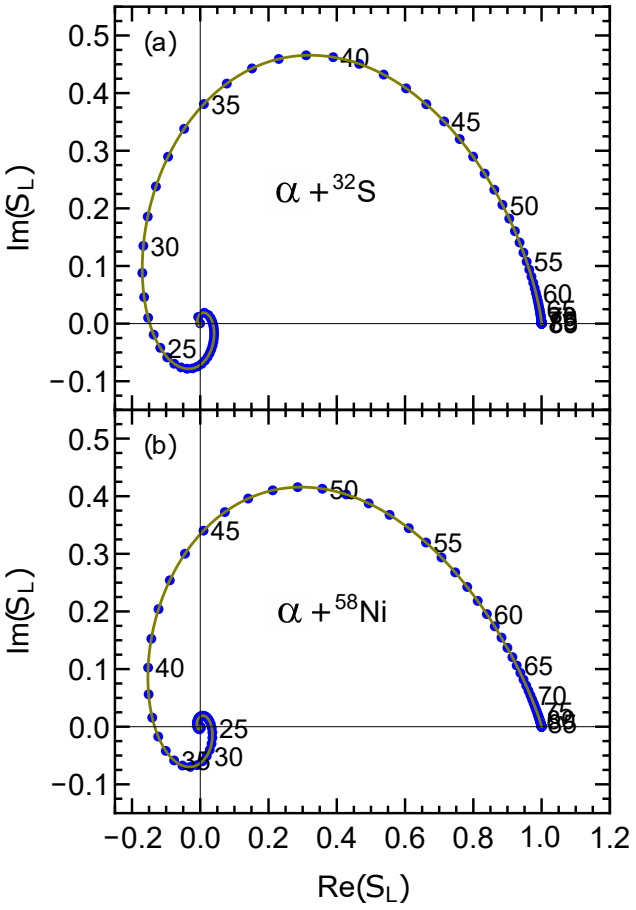

Fig. 3. (Color online) Argand diagram of the scattering matrix element for $\alpha + {}^{32}$S and $\alpha + {}^{58}$Ni elastic scatterings at 386 MeV. The Arabic numerals along the curve denote the $L-$values.

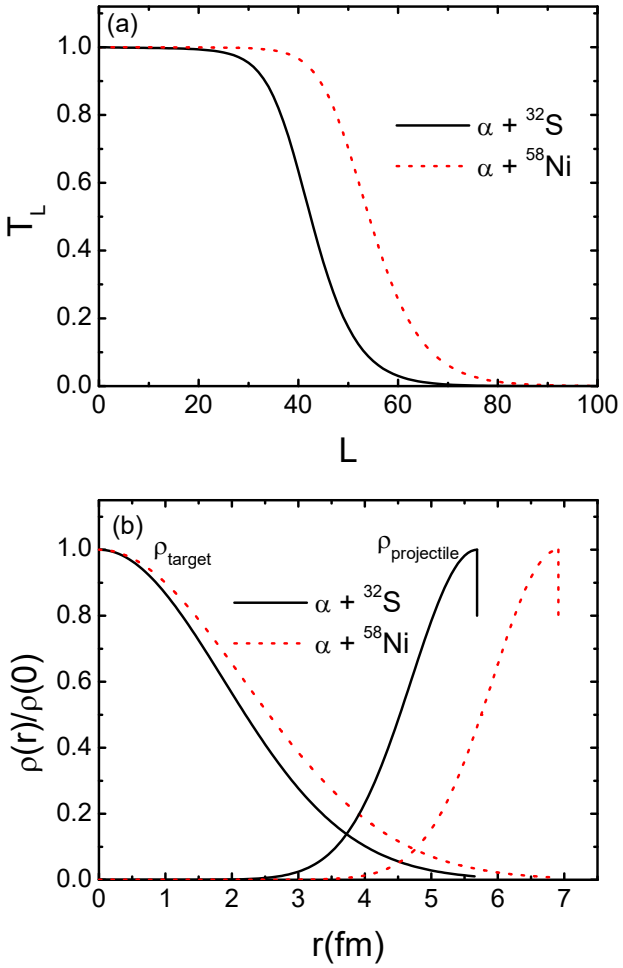

Fig. 4. (Color online) (a) Transmission functions, and (b) density overlaps of two colliding nuclei when the distance between two nuclear centers is equal to R_s for $\alpha + {}^{32}$S and $\alpha + {}^{58}$Ni systems at 386 MeV.

get mass increases, the R_s increases, and thus the σ_R (or σ_{R_s}) increases.

The overlaps of the projectile and target densities are shown in Fig. 4(b) when the distance between the centers of the two colliding nuclei is equal to the R_s. In this figure, it is assumed that both the projectile and the target have a Gaussian-shaped density distribution given by :

$$\rho(r) = \rho(0)\exp(-\frac{r^2}{a^2}), \quad a = \frac{R_{\rm rms}}{\sqrt{1.5}}, \tag{11}$$

where root-mean-square radii ($R_{\rm rms}$) were taken as 1.71 fm for ^{4}He, 3.243 fm for ^{32}S and 3.764 fm for ^{58}Ni taken from Ref. 16. The overlap provides an interpenetration of the two colliding nuclei with a fixed absorption rate ($T_L = 1/2$) for two scattering systems. As Fig. 4(b) shows, the density overlap of two colliding nuclei for $\alpha +$ ^{32}S system is larger than the one for $\alpha + {}^{58}$Ni system, indicating weak absorption. This weakening absorption allows colliding nuclei to interpenetrate more deeply without being absorbed. Consequently, the σ_R of $\alpha + {}^{32}$S system is smaller than the one of $\alpha + {}^{58}$Ni system.

3. Potential radius parameter effect on differential and reaction cross sections

To investigate how variations in real (r_v) and imaginary (r_w) radius parameters of WS potential affect the differential cross section, we plotted the $d\sigma/d\sigma_{\rm Ruth}$ of $\alpha + {}^{32}$S system by varying the r_v (or r_w) value, where the other potential parameters except r_v (or r_w) were fixed.

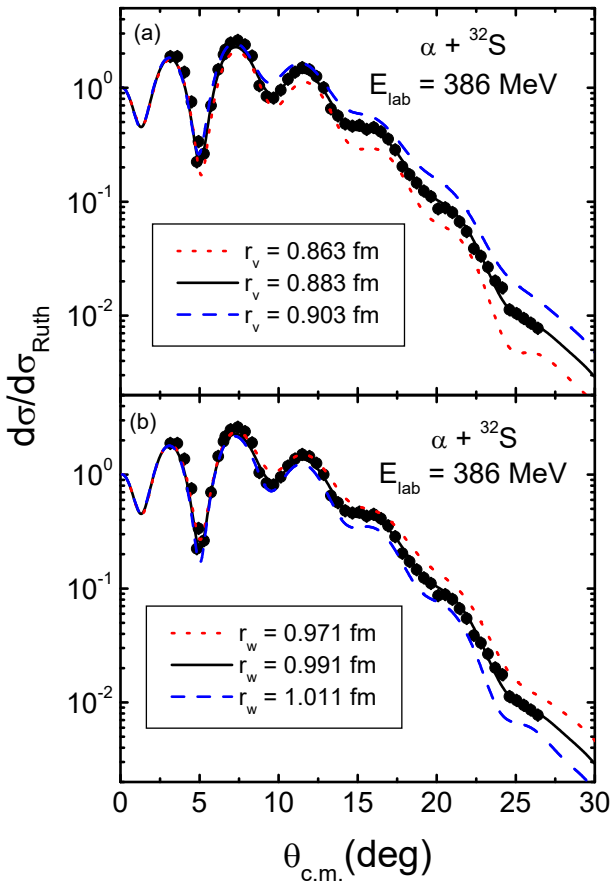

Fig. 5. (Color online) Angular distributions for $\alpha + {}^{32}$S elastic scattering at 386 MeV calculated using different real (or imaginary) radius parameters r_v (or r_w). Other input parameters in the angular distribution calculation were fixed, and these values are given in Table 1.

The radius parameters are taken ± 0.02 fm from r_v (or r_w) value given in Table 1, and the calculation results using the tangential velocity at r_c are plotted in Fig. 5. As this figure shows, in the relatively large angle region, the $d\sigma/d\sigma_{\rm Ruth}$ move upward (downward) as the value of r_v increases (decreases). On the other hand, an increase (decrease) in the value of r_w shifts the $d\sigma/d\sigma_{\rm Ruth}$ downward (upward). In both Figs. 5(a) and 5(b), the three curves show that the difference becomes larger as the $\theta_{\rm c.m.}$ increases.

The T_L function can be expressed as $T_L = 1 - \exp[-4{\rm Im}(\delta_L)]$ with the help of Eq. (2) because the phase shift δ_L is given in complex form as $\delta_L = {\rm Re}(\delta_L) + i{\rm Im}(\delta_L)$. Meanwhile, as given in Eq. (10), the reaction cross section σ_R is related to the T_L function obtained from the ${\rm Im}(\delta_L)$. Therefore, the σ_R is directly related to the ${\rm Im}(\delta_L)$. As given in Eqs. (7)–(9), the ${\rm Im}(\delta_L)$ is obtained from the imaginary part of WS potential (${\rm Im}(U(r))$), so the σ_R is ultimately affected by the ${\rm Im}(U(r))$. Three different r_w values produce somewhat different σ_R values (σ_R = 1016 mb, 1052 mb and 1089 mb for r_w = 0.971 fm, 0.991 fm and 1.011 fm, respectively) in $\alpha + {}^{32}$S system. It can be seen that the σ_R value increases as the imaginary radius parameter r_w increases.

IV. CONCLUDING REMARKS

This paper presented the results of eikonal model analysis for the measured data of 386 MeV $\alpha-$particle elastic scattering from ^{32}S and ^{58}Ni targets. For model calculation, the WS potential with six-parameters and the tangential velocity at r_c are used. The calculation results successfully reproduced the structure of experimental angular distribution and were in good agreement with the measured data. Strong interference between near- and far-side scattering amplitudes is thought to give rise to the oscillatory structures that appears around the crossing angle in the angular distribution. In the regions of scattering angle greater than crossing angle, the far-side amplitude made an important contribution in determining the behavior of the elastic cross section.

The graphical images of scattering matrix elements S_L of two systems show similar shapes and display two distinct characteristics: the first one is that they begin at (Re(S_L), Im(S_L)) = (0.0, 0.0) and end at (1.0, 0.0) ; the other is that the graphical images look like a nautilus shell spiral. The critical angular momentum $L_{1/2}$ and the strong absorption radius R_s for ^{32}S target are smaller than those for ^{58}Ni target. The geometric reaction cross section σ_{R_s} can be extracted from the R_s in terms of $\sigma_{R_s} = \pi R_s^2$, and its values are comparable to the reaction cross sections σ_R obtained using partial wave sum. The fact that the σ_{Rs} and σ_R values are similar indicates that R_s can be usefully used to estimate the magnitude of σ_R. When two colliding nuclei are separated by R_s, projectile and target densities are found to overlap more in $\alpha + {}^{32}$S system than $\alpha + {}^{58}$Ni case, indicating weak absorption. As a result, the σ_R value of $\alpha + {}^{32}$S system is smaller than that of $\alpha + {}^{58}$Ni system.

As the value of real radius parameter r_v of WS potential increases (decreases), the elastic cross section moves

upward (downward), especially in the relatively large angle regions. On the other hand, increasing (decreasing) the imaginary radius parameter r_w value shifts the elastic cross section downward (upward). Additionally, as r_w increased, the reaction cross section also increased.

ACKNOWLEDGEMENTS

This research was supported by the 2024 scientific promotion program funded by Jeju National University.

REFERENCES

[1] D. Waxman, C. Wilkin, J.-F. Germond and R. J. Lombard, Eikonal Corrections for Spin-Orbit Potentials, Phys. Rev. C **24**, 578 (1981).

[2] F. Carstoiu and R. J. Lombard, Eikonal Expansion for Total Cross Sections of Heavy Ion Reactions, Phys. Rev. C **48**, 830 (1993).

[3] M. H. Cha and Y. J. Kim, Higher-Order Corrections to the Eikonal Phase Shifts for Heavy-Ion Elastic Collision, Phys. Rev. C **51**, 212 (1995).

[4] A. Ingemarsson, Effects of Refraction on Absorption in the Scattering of Lighter Heavy Ions, Phys. Rev. C **56**, 950 (1997).

[5] C. E. Aguiar, F. Zardi and A. Vitturi, Low-Energy Extensions of the Eikonal Approximation to Heavy-Ion Scattering, Phys. Rev. C **56**, 1511 (1997).

[6] Y. J. Kim and M. H. Cha, Second-Order Eikonal Model Analysis of ^{16}O + ^{16}O Elastic Scattering, Int. J. Mod. Phys. E **10**, 373 (2001).

[7] Y. J. Kim, J. K. Woo and S. J. Lee, Eikonal Model Analysis of 240 MeV ^{6}Li Elastic Scattering on ^{24}Mg and ^{28}Si, J. Korean Phys. Soc. **60**, 1477 (2012).

[8] C. Hebborn and P. Capel, Analysis of Corrections to the Eikonal Approximation, Phys Rev. C **96**, 054607 (2017).

[9] B. Bonin *et al.*, Alpha-Nucleus Elastic Scattering at Intermediate Energies, Nucl. Phys. A **445**, 381 (1985).

[10] H. L. Clark, Y.-W. Lui and D. H. Youngblood, Alpha Particle Optical Potentials at 240 MeV, Nucl. Phys. A **589**, 416 (1995).

[11] B. K. Nayak *et al.*, "Bi-modal" Isoscalar Giant Dipole Strength in ^{58}Ni, Phys. Lett. B **637**, 43 (2006).

[12] M. Itoh *et al.*, Isoscalar Giant Resonance Strengths in ^{32}S and Possible Excitation of Superdeformed and ^{28}Si + α cluster bandheads, Phys. Rev. C **88**, 064313 (2013).

[13] F. Alqahtani and A. A. Ibraheem, Study of α+^{32}S Scattering Using Different Potentials at 386 MeV, Indian J. Phys. **95**, 499 (2021).

[14] D. M. Brink, *Semi-Classical Methods for Nucleus-Nucleus Scattering* (Cambridge University Press, Cambridge, 1985), Chap. 2, p. 6.

[15] R. C. Fuller, Qualitative Behavior of Heavy-Ion Elastic Scattering Angular Distributions, Phys. Rev. C **12**, 1561 (1975).

[16] C. W. de Jager, H. de Vries and C. de Vries, Nuclear Charge- and Magnetization-Density-Distribution Parameters from Elastic Electron Scattering, At. Data Nucl. Data Tables **14**, 479 (1974).